# Bone marrow dosimetry for mice: exposure from bone-seeking 89,90Sr

**Elena Shishkina** ( elenaa.shishkina@gmail.com )
Chelyabinsk State University
**Alina Shuiskaya**
Chelyabinsk State University
**Pavel Sharagin**
Urals Research Center for Radiation Medicine

**Research Article**

**Keywords:** dosimetric modeling, computational phantoms, mouse-like rodents, internal exposure, bone marrow, Sr isotopes

**Posted Date:** June 24th, 2022

**DOI:** https://doi.org/10.21203/rs.3.rs-1760833/v1

# Bone marrow dosimetry for mice: exposure from bone-seeking $^{89,90}$Sr

**Elena Shishkina[1,2], Alina Shuiskaya[1], Pavel Sharagin[2]**

[1] Chelyabinsk State University, 129 Bratiev Kashirinykh Str., 454001, Chelyabinsk, Russia
[2] Urals Research Center for Radiation Medicine, 68A, Vorovsky Str., 454124, Chelyabinsk, Russia

Corresponding author: Elena Shishkina, elenaa.shishkina@gmail.com

**ORCID:**

Elena Shishkina - 0000-0003-4464-0889

Pavel Sharagin - 0000-0002-1457-4916

**Abstract:** Studies of radiobiological effects in murine rodents exposed to internal radiation in the wild or in laboratory experiments require a dosimetric support. The main problem of bone marrow (BM) dosimetry for bone-seeking β-emitters is dosimetric modeling due to the fact that the bone is a heterogeneous structure with complex microarchitecture. To date, there are several approaches to calculating the absorbed dose in BM, which mostly use rough geometric approximations. Recently, in the framework of studies of people exposed to $^{90}$Sr in the Urals, a new approach (*SPSD*) has been developed. The aim of current study was to pilot test the possibility of extension of the *SPSD*-approach elaborated for humans to mice. The computational phantoms of femur bones of laboratory animals (*C57BL/6*, *C57BL/6J*, *BALB/c*, *BALB/cJ*) aged 5-8 weeks (growing) and >8 weeks (adults) were created. The dose factors to convert the $^{89,90}$Sr activity concentrations in a bone tissue into units of the dose rate absorbed in the bone marrow were estimated as follows: $DF_{Sr\text{-}90(BM \leftarrow TBV+CBV)}$ is equal to 1.75±0.42 and 2.57±0.93 (μGy day$^{-1}$) per (Bq g$^{-1}$) for growing and adults, respectively; $DF_{Sr\text{-}89(BM \leftarrow TBV+CBV)}$ is equal to 1.08±0.27 and 1.66±0.67 (μGy day$^{-1}$) per (Bq g$^{-1}$) for growing and adults, respectively. These results are about 2.5 times lower than skeleton-average *DF*, calculated assuming the homogenous bone, where source and target coincide. The study demonstrates the possibility of application of the *SPSD*-approach elaborated for humans to non-human mammals.

**Key words:** *dosimetric modeling, computational phantoms, mouse-like rodents, internal exposure, bone marrow, Sr isotopes.*

**Statements and Declarations**

The authors have no relevant financial or non-financial interests to disclose.

The authors did not receive support from any organization for the submitted work.

The authors have no competing interests to declare that are relevant to the content of this article.

All authors certify that they have no affiliations with or involvement in any organization or entity with any financial interest or non-financial interest in the subject matter or materials discussed in this manuscript.

## Author Contributions Statement

Elena Shishkina and Alina Shuiskaya wrote the main manuscript text. Elena Shishkina provided conceptualization and supervision. Alina Shuiskaya performed investigations. Pavel Sharagin performed calculations and prepared figure 1. All authors reviewed the manuscript.

## Introduction

Strontium beta-emitting isotopes ($^{90}$Sr and $^{89}$Sr) fall into the environment as a result of anthropogenic radiation events that may lead to significant consequences for humans and biota. Large amounts of Sr isotopes were released and globally dispersed due to atmospheric weapons testing in the mid of the last century (Povinec et al. 2005). Some local territories were also contaminated accidentally. For example, the vast territories of Russia, Belorussia and Ukraine were contaminated with long-lived $^{90}$Sr (~29 years) due to the Techa River releases (Degteva et al. 2016), Kyshtym accident (Izrael 2013) and Chernobyl accident (Askbrant et al. 1996). Solubility of Sr results in its high *bio*-accessibility through food chains. Stable strontium is a low toxicity element. However, bone-seeking beta-emitters may be adverse for hematopoietic and mesenchymal stem cells surrounded by bone structures. Long-lived $^{90}$Sr ($T_{1/2}$~29 years) may irradiate the active bone marrow over a long period of time. Adverse health effects of chronic radiation exposure for small mammals are highly debated topic (Fesenko 2019; Dahl et al. 2021; Shishkina et al. 2021a).

Internal radiation dosimetry for animals is an important issue of radiation research. There are several approaches to dosimetric modeling. The first one was elaborated in the framework of ICRP system of environmental protection (ICRP 2008). It is quite conservative and based on a set of principles, viz.: 1) simplified representation of exposure geometry (elliptic body shape); 2) uniform radionuclide distribution within homogeneous body media; 3) absorbed dose averaged over the whole body. The second approach is used in order to support the animal experiments of chronic radionuclide intakes (Bitar et al. 2007; Keenan et al. 2010; Locatelli et al. 2017). The realistic voxel-based three-dimensional computer models of mice and rats of different sex and age allow calculating the doses from selected source or target pairs (cross-organ doses). The second approach has a *great advantage* of being combined with biokinetic models, and allows obtaining the accurate organ-specific doses. However, existing realistic animal models describe the skeleton as a homogeneous medium and do not take into account the bone microstructure. Doses in active marrow exposed to bone-seeking beta emitters, such as $^{89}$Sr or $^{90}$Sr/$^{90}$Y (energies of electron emission are 0–1.5 MeV and 0–2.4 MeV, respectively), should be calculated considering both macro- and microstructures of bones (Shishkina et al. 2021b). The description of spongy bone microarchitecture as well as separation of the source and target (bone and bone marrow) are important because the fraction of energy absorbed in spongiosa is deposited withing the bone outside the bone marrow volume.

Advanced methods for human bone dosimetry are based on combinations of ex vivo computed tomography (CT) images and micro-CT (*μ-CT)* or nuclear magnetic resonance micro-images of trabecular bone (Kramer et al. 2012; Zankl et al. 2018). This approach provides a highly realistic model of a scanned bone. However, the dimensions of a separate bone may differ from the population-average sizes. Moreover, the image-based computational phantom is non-parametric and does not allow for the estimation of uncertainties associated with individual variability of bone morphology. The Stochastic Parametric Skeletal Dosimetry (*SPSD*) approach (Degteva et al. 2021), which was originally proposed by Shishkina et al. (2018) and Zalyapin et al. (2018) is an alternative, which allows for the generation of models based on population average, sex- and age-specific morphometric data. The parametric approach allows creating a set of random models reflecting the individual variability of bone micro and macro dimensions. Computational phantoms are generated by software *«Trabecula»* (Shishkina et al. 2020) as figures of simple geometric shape (Sharagin et al. 2018). Phantoms consist of a spongiosa, where rod-like bone trabeculae penetrate the bone marrow, and a cortical bone layer covering it. The parameters to generate a phantom are as follows: 1) macro-parameters include linear bone dimensions and cortical thickness (*Ct.Th*); 2) micro-parameters of spongiosa include trabecular thickness (*Tb.Th*), trabecular separation (*Tb.Sp*) and bone volume fraction (*BV/TV*). The human-specific parameters were evaluated based on literature analysis in Sharagin et al. (2021) and Tolstykh et al. (2021). Similarly, a vast amount of morphometric information on bone-specific

micro- and macro-dimensions for mice is available in the published papers and could be used for parameterization of murine-specific computational phantoms for bone dosimetry.

The aim of current study was to pilot test the possibility of extension of the *SPSD*-approach elaborated for humans to non-human mammals. Mice, which belong to the reference animals typical of terrestrial ecosystems and could be used as a convenient model for understanding the "exposure–dose" and "dose-effect" dependencies, were chosen as the object of the study. One of the main hematopoietic sites of the adult murine skeleton is limb bones comprising from 20 to 35% of total active marrow (Shaposhnikov 1979; Boggs 1984; Epp et al. 1959; Taketa et al. 1970). Since the most of bone microarchitecture measurements are available for experimental animals, we collect the published research data on femur micro- and macro-dimensions for laboratory mice of different strains. Based on the parameters derived from the literature, the set of computational phantoms was generated and used for estimation of dose factors, converting the specific activity of $^{90}$Sr and $^{89}$Sr incorporated in cortical and trabecular bone volumes to dose rate in active marrow.

## Materials and methods

### Creation of computational phantom of murine femur

The shape of femur bone is simplified with cylindrical approximation (Fig. 1). The height ($l$) and diameter ($d$) of the cylinder are assumed to be equal to the most commonly used morphometric indices, viz., maximum length of the femur ($L$), which is the distance from the greatest trochanter to the medial condyle, and the diameter ($D$), which is the width of bone in the middle of diaphysis. The thickness of cortical layer ($\widehat{Ct.Th}$) (it covers the lateral cylindrical surface only) is assumed to be uniform and equal to the average *Ct.Th* of the bone. Parameters of bone microstructure, viz., trabecular thickness ($\widehat{Tb.Th}$), trabecular separation ($\widehat{Tb.Sp}$) and bone volume fraction ($\widehat{BV/TV}$), correspond to histomorphometry parameters (*Tb.Th, Tb.Sp* and *BV/TV*) of standard nomenclature (Bouxsein et al. 2010).

Collection of published data on morphometric studies was based on the following criteria:

- original papers only were considered;
- only studies of "healthy" bones were accepted (without fractures, diseases or drugs that lead to damage to bone structures);
- only studies with a well-described experiment (strains, amount, sex and age, animal housing conditions and diet) were considered;
- results obtained under similar condition were included (no extreme diet or temperature or any other factors of influence);
- all measurements on macro-dimensions (*L, D*) obtained with CT, microscopy or caliper were accepted;
- histomorphometry results (*Ct.Th, Tb.Th, Tb.Sp* and *BV/TV*) obtained with microscopes or $\mu$-*CT* with method resolution $< 70$ μm were accepted.

Totally, 33 papers met these criteria. The following information was derived: 1) strain; 2) sex; 3) age; 4) sample size; 5) data available on one or several dimensions, such as *L, D, Ct.Th, Tb.Th, Tb.Sp* and/or *BV/TV*; 6) individual variability of the dimensions (if available) in terms of standard deviation; 7) reference.

The collected results comprise both male and female data and are related to mice of 2 wild types, 16 inbred strains of laboratory animals, as well as 1 publication summarizing bone microarchitecture data on 62 strains of inbred mice. All literature derived data are presented in the Supplementary Information file (Supplementary Information.xlsx).

The bone dimensions of mice of different sex and strains were compared (Spearman correlation with α=0.05, Mann–Whitney U test with α=0.05) to decide whether it is possible to pool the data together for combined analysis.

The weighted averaging of morphometric dimensions ($x_i$) of different sample size ($n_i$) derived from publication $i$ was done according to Eqn. (1):

$$\hat{x} = \sqrt{\frac{\sum_{i=1}^{N} x_i * n_i}{\sum_{i=1}^{N} n_i}};\ \sigma_{\hat{x}} = \sqrt{\frac{\sum_{i=1}^{N} (x_i - \hat{x})^2}{N-1}}, \quad (1)$$

where $\hat{x}$ – a model parameter; $\sigma_{\hat{x}}$ – uncertainty of $\hat{x}$; $N$ – total number of information sources.

The individual variability of parameter $\hat{x}$ was calculated as a propagation of weighted average individual variabilities ($\sigma_{x_i}$) and non-excluded systematic error of $\hat{x}$ equal to $\sigma_{\hat{x}}$ (Eqn. 2).

$$\hat{\sigma}_{\hat{x}} = \sqrt{\left(\frac{\sum_{i=1}^{N} \sigma_{x_i} * n_i}{\sum_{i=1}^{N} n_i}\right)^2 + (\sigma_{\hat{x}})^2} \quad (2)$$

The obtained estimates of the parameters and their individual variability were used as an input data for computational phantom generation in the *«Trabecula»* software (Shishkina et al., 2020). Another input data to create *SPSD* model is the intra-specimen variability of the trabecular thickness and the trabecular separation. We have not found any description of the intra-specimen variability of these parameters in mouse bones in the available literature. The values of the variation coefficients typical of human bones (as it was presented in Supporting materials S1 to Degteva et al. 2021) were used as a surrogate, namely, 22% and 23% for $\widehat{Tb.Th}$ and $\widehat{Tb.Sp}$, respectively. The computational phantom with average dimensions ($\hat{\boldsymbol{x}}$) and 12 random variative models (within $\pm\hat{\boldsymbol{\sigma}}_{\hat{\boldsymbol{x}}}$) were generated using the software *«Trabecula»*. The software automatically calculates the volumes of source and target tissues for each of the generated phantoms.

**Monte-Carlo simulations of radiation transport**

Each set of phantoms was used for Monte-Carlo simulation of electron and photon transport within the bone and bone marrow media to calculate the energy deposition ($E_r\ (BM \leftarrow S)$) in bone marrow (*BM*) per decay of Sr isotopes ($r$ –radionuclide considered) uniformly distributed in cortical or trabecular bone media ($S$ –the source tissues). Probability of electron emission of different energies for $^{89}$Sr, $^{90}$Sr and $^{90}$Y decays were taken from the Atomic Data Information System – *«Janis 4.1»* (Java - based Nuclear Data Information System) (Soppera 2014), available in the public domain. The decays of $^{90}$Sr and its progeny $^{90}$Y computed with equal probability (simulating the secular equilibrium) and the overall energy deposition was calculated per mother's radionuclide decay. Elemental composition of simulated media was assumed to be the same as for humans (Table. 1) (ICRP89 2002). In contrast to the chemical composition, the murine bone density is lower than that typical of humans (1.64 – 1.89 r/cm$^3$) and it has been taken as 1.57 g/cm$^2$ (Broulík et al. 2013).

Radiation transport was imitated using *«MCNP 6.2»* (Monte - Carlo N - Particle Transport Code). The number of histories was at least 4000000; statistical error < 1%.

**Calculation of absorbed dose rate in the bone marrow of murine femur**

Dose factors ($DF_r(BM \leftarrow S)$) to convert the radionuclide specific activity in a source-tissue into units of the dose rate absorbed in the *BM* were calculated by normalization of the energy deposition per decay according to Eqn. (3):

$$DF_r(BM \leftarrow S) = E_r\ (BM \leftarrow S) * \frac{m_S}{m_{BM}}, \quad (3)$$

where $m_S$ is the mass of a source tissue; $m_{BM}$ is the mass of the target tissue.

Total dose rate in *BM* can be expressed by Eqn. (4).

$$\dot{D}_r = A_r(CBV) \times DF_r(BM \leftarrow CBV) + A_r(TBV) \times DF_r(BM \leftarrow TBV), \quad (4)$$

where $\dot{D}_r$ is the dose rate in *BM*; $A_r(CBV)$ and $A_r(TBV)$ are the radionuclide (*r*) activity concentration in the cortical (*CBV*) and trabecular (*TBV*) bone volumes, respectively. Assuming the uniform radionuclide distribution in the whole bone media ($A_r(CBV) \approx A_r(TBV) = A_r$) the overall dose rate per 1 Bq g$^{-1}$ was calculated with Eqn (5).

$$DF_r(BM \leftarrow CBV + TBV) = A_r \times \left(DF_r(BM \leftarrow CBV) + DF_r(BM \leftarrow TBV)\right), \quad (5)$$

## Results

### Creation of computational phantom of murine femur

Macro dimensions (*L* and *D*) did not correlate with murine strains. This allows combining all literature-derived macro dimensions (14 papers describing >500 animals). However, Spearman correlation analysis showed the statistically significant relationship ($P < 0.05$) between the mouse strain and all microarchitecture measurements (*BV/TV, Tb.Th, Tb.Sp*, Ct.Th). Wherein no statistically significant difference in micro dimensions was found for *C57BL/6*, *C57BL/6J*, *BALB/c*, *BALB/cJ*. Therefore, the laboratory animals of these strains were selected as a modeling subject. It should be noted that the greatest number of studies are devoted exactly to the strains selected. Totally 15 papers describing different morphometric parameters of >350 mice were considered for spongiosa microarchitecture modeling. Table 2 summaries the statistics of the data available from papers about microarchitecture. No statistically significant relationships between the microarchitecture dimensions and sex were found. Therefore, the computational phantoms were constructed without sex differentiation. However, the age-related changes in bone dimensions were considered.

All data on animals of different age can be conventionally divided into 3 groups: juvenile (≤5 weeks), growing (5 - 8 weeks) and adult (>8 weeks). As it can be seen from Table 2, not many papers on microparameters were related to the juveniles. The data on femur length (*L*) described the growing and adult animals mainly. For example, minimal age of animals with measured *L*, which were studied in parallel with microparameters (Table 2), is 4 weeks old. Data on femur diameters were found for adults only (Dubrovsky at al. 2020). Therefore, the femur computational phantoms were created for growing and adult mice only and femur diameter of the growing mouse was assumed to be equal to that of an adult as a first approximation.

Mean values of *Tb.Th, Tb.Sp* and *BV/TV* were almost equal in the age groups. However, the individual variability was about twice higher in adults. *Ct.Th* increases with age up to 24 weeks (Papageorgiou et al., 2020). Therefore, both *Ct.Th* and corresponding individual variability were twice higher in adults. Table 3 shows the parameters estimated based on morphometric data for femur phantoms of growing and adult laboratory animals.

As a result, two sets of computational phantoms were generated for two age groups. Each one comprises one model with average group parameters (basic phantom) and 12 randomly generated models to simulate the individual variability of bone dimensions (supplementary phantoms). Phantoms were used for dose factor calculations.

### Dose factors

Table 4 presents the dose factors calculated for $^{90}$Sr (in equilibrium with $^{90}$Y) and $^{89}$Sr incorporated in *TBV* and *CBV* to convert the radionuclide specific activity into the dose rate in the *BM*. The results are shown as a central estimate (calculated with basic phantom) ± root mean square deviation (*rmsd*) of twelve $DF_r(BM \leftarrow S)$ obtained using

supplementary phantoms from that obtained with the basic one. The *rmsd* reflects the effect of individual variability of bone dimensions.

According to Table 4, the dose rate formed by one Bq $g^{-1}$ of Strontium isotopes in *TBV* of adults is about 20% lower than that of growing mice. This is a combined effect of slightly lower bone fraction of spongiosa (*BV/TV*) for adults and greater spongiosa surface (66 $mm^2$ versus 57 $mm^2$), which increases the probability of energy loss from spongiosa volume. On the contrary, $DF_r(BM \leftarrow CBV)$ of adults is about two times higher than that of growing. This is the effect of 2 times higher $\widehat{Ct.Th}$ in adult's phantom. The difference in cortical thickness led to the difference in source-tissue volume and, as a result it changed the $\frac{m_S}{m_{BM}}$ ratio (Eqn. 3). The variability of *DFs* does not exceed 64% for *S=TBV* and 22% for *S=CBV*.

Individual variability of *BV/TV* (proportional to spongiosa density) is quite high (Table 3): 38% and 75% for growing and adults, respectively. As a result, the uncertainties of $DF_r(BM \leftarrow TBV)$ were about the same. In addition to *BV/TV,* individual variability of *Ct.Th* is an important factor of influence on $DF_r(BM \leftarrow CBV)$ uncertainty. Variability of *Ct.Th* for growing and adults is equal to 22% and 42%, respectively. The combined effect results in $DF_r(BM \leftarrow CBV)$ uncertainty of 38% and 66% respectively.

Separation of the trabecular and cortical bones as source-tissues can be useful when combining a dosimetric model with a biokinetic one that takes into account the difference in remodeling of these two types of bones. However, today's biokinetic models for rodents do not distinguish the cortical and trabecular bones (Malinovsky et al. 2013) and the doses are calculated assuming uniform radionuclide distribution within all bone structures. Therefore Table 4 includes the dose factors of combined *CVB+TBV* source. The overall uncertainties of the estimates are about 25% and 40% for growing and adults, respectively.

## Discussion

### Dose factors calculated with different approaches.

Dose calculation can be done with different accuracy and precision depending on the specific task. For example, the radiological protection commonly requires conservative estimate for a reference animal. However, radiobiological and medical studies need accurate individual doses. We have compared the SPSD-based dose factors and the estimates with conservative approach implemented in the *ERICA Tool 2.0* (Brown et al. 2016) as well as with calculations performed using the software for radiobiological studies *RODES VI* developed by IRSN (Locatelli et al. 2017). The Erica Tool was elaborated to support decision-making on environmental issues related to the ionizing radiation effect with emphasis on ensuring the structure and functioning of ecosystems. On the contrary, the *RODES VI* software was created to support animal experiments on chronic radionuclides intake. Within the *ERICA Tool* 2.0, a body is assumed to have a spheric/ellipsoid shape with homogeneous medium containing uniformly distributed radioactivity. In other words, both body heterogeneity and the strontium bone-seeking nature are ignored. The *RODES VI* uses voxel-based three-dimensional computer models of mice and rats, which were developed based on magnetic resonance imaging. This software is aimed to be realistic. However, it also uses some simplifications, such as an assumption of bone homogeneity. Mean absorbed energy has been calculated for the whole uniformly contaminated skeleton. In other words, the source (bone) and target (*BM*) are not separated.

Table 5 presents the results of the comparison of dose factors calculated with different approaches for adults due to incorporated $^{89,90}$Sr. The source tissue is indicated as *S*; the target is indicated as *T*. *Erica Tool 2.0* calculates the body-

average dose (we "create" an body with dimensions 8.9x2.5x2.5 cm and m= 20.5 g). Using *RODES VI* we calculated the skeleton-average dose for mice with body mass m=20g.

As it can be seen from the table, *ERICA* conservative integrated approach is not appropriate for internal *BM* dosimetry. Estimating the body-average radionuclide activity concentration based on bone measurements requires an additional information on intakes and biodistribution. A rough extrapolation of radionuclide bone burden to the whole body and whole-body dose to BM dose could lead to a 5-fold overestimate.

Neglecting the bone microstructure and calculating average energy absorption in the skeleton (*RODES VI*) leads to an overestimation of the dose to the bone marrow by a factor of 2.5. The skeleton dose rates calculated using *RODES VI* cannot be propagated to BM either; they do not fall within the 90% confidence intervals of *SPSD*-based results. This example illustrates the importance of taking into account the microstructure in evaluation of internal exposure of *BM* to bone-seeking beta-emitting radionuclides. It should be noted, that the authors of *RODES* software indicate this problematic issue as a further direction of the software improvement (Locatelli et al. 2017).

**Dosimetry of rodents exposed at the East Urals Radioactive Trace**

Vast territories of the Urals were contaminated due to long-lived $^{90}$Sr released as a result of a thermal explosion of a storage tank of radioactive waste in the territory of the Mayak Production Association, Russia (the so-called Kyshtym accident) (Avramenko et al. 1997; Izrael 2013) on 29 September 1957. Radionuclides were deposited on the soil surface forming the East Urals Radioactive Trace (EURT). It led to a radiation exposure of the inhabitants of these territories, rodents among them. Despite the fact that more than 60 years (about two half-lives of $^{90}$Sr) have passed since the radiation accident, a large part of the EURT territory is still heavily contaminated. For example, in 2001-2012 the local concentration of $^{90}$Sr in a 10 cm layer of the soil reached 20 Bq g$^{-1}$ (Molchanova et al. 2009; Molchanova et al. 2014; Mikhailovskaya et al. 2019). Many studies of radiation effects in EURT rodents have already been published (Ilyenko 1974; Gileva 2002; Orekhova and Modorov 2017; Orekhova et al. 2019) and continue to be carried out. The data on radiation effects should be supported by radiation dosimetry. Internal *BM* exposure due to $^{90}$Sr incorporation can be based on the information about skeleton contamination (Starichenko 2004; Starichenko et al. 2014). In Shishkina et al. (2021a) the data on $^{90}$Sr skeleton contamination of herb field mouse (*Sylvaemus uralensis*) obtained during long-term (2003 – 2012 years) study were summarized. There were 3 sampling areas selected for the purposes of the study with the following initial (just after the explosion) $^{90}$Sr deposition density: (1) 3.7-37 MBq m$^{-2}$; (2) 74-3,700 kBq m$^{-2}$ and (3) 37 kBq m$^{-2}$. The data on *subadultus* (non-breeding underyearlings) can be roughly associated with the data on growing individuals; two groups of breeding individuals (underyealing and wintering) can be associated with adults in the current study. Table 6 presents the group-average data on $^{90}$Sr activity concentration in the murine bones (per wet weight) estimated according to Shishkina et al. (2021a) and the corresponding *BM* dose rates. The 90%CI for the dose rate reflects the overall individual variability of the activity concentrations and dose factors. The overall variation coefficients were calculated with the uncertainty propagation law; 90%CI was estimated using the lognormal approach.

In the wild, the mean life span of a mouse-like rodent is about 1.5 years. The cumulative internal dose in the rodent bone marrow estimated with *SPSD*-approach amounts to ~70 mGy and does not exceed 120 mGy in the EURT territories with 3.7 -37 MBq m$^{-2}$ of surface contamination.

Taking into account the non-uniform distribution of bone-seeking $^{90}$Sr in organism, the maximum organ dose is formed in bone tissue and bone marrow. The remaining tissues are exposed to a lesser extent. Therefore, the results obtained could be considered as a conservative estimate of whole-body dose rates to be compared with a screening value (the dose rate threshold that does not lead to an unacceptably high level of risk of the effect on the structure and function

of the ecosystem). The chronic exposure screening value of 240 μGy day$^{-1}$ was established in Erica Assessment Tool (Brown et al. 2016) based on the analysis of the chronic exposure data from more than 26,000 data entries in the original Fine-Root Ecology Database (FRED) (Iversen et al. 2017). Dose rates estimated with *SPSD*-based approach are significantly lower than the screening level.

To compare this result with commonly accepted approach implemented in the *ERICA Tool 2*, we have to convert the bone-specific activity concentration of $^{90}$Sr to body-average value. The biokinetic model of $^{90}$Sr (Malinovsky et al. 2013) for adult mouse has been used to calculate the soft tissue exposure assuming the chronic intake and steady state between the organism and environment. The soft tissue activity should be 0.162 times lower than the bone burden. Assuming the mass fraction of skeleton as 13% of total body weight (Malinovsky et al. 2013), the 1 Bq g$^{-1}$ of $^{90}$Sr in bone tissue corresponds to 0.27 Bq g$^{-1}$ of body-average activity concentration. Therefore, to calculate the body-average dose rate based on given $^{90}$Sr activity concentration in bones a dose factor should be used: $0.27 * DF_{Sr-90}(whole\ body \leftarrow whole\ body) = 3.48$ (μGy day$^{-1}$)/ (Bq g$^{-1}$ of bone wet weight). Whole body doses in this case would be 1.8 times higher than the bone marrow SPSD doses shown in Table 6. Even with this conservative approach, mean dose rates in the sampling areas do not exceed 200 μGy day$^{-1}$. The upper dose bounds of 90% CI calculated for the area with maximum contamination level can reach 290 μGy day$^{-1}$. In other words, both the conventional approach in radiation protection and the SPSD-based bone marrow dose estimates do not, on the average, exceed the screening level.

And on the contrary, the use of the approach of homogenous spongiosa (*RODES VI*) for dose prediction provides the values comparable with the screening value in the most contaminated area (3.7-37 MBq m$^{-2}$): mean dose rate is ~240 μGy day$^{-1}$ (up to 400 μGy day$^{-1}$). The homogenous spongiosa approach has been used for murine-specific internal dosimetry in a number of EURT studies (Malinovsky et al. 2014; Modorov 2014) using dose factors estimated by Chesser et al. (2000) and calculations based on Stabin et all (2006) which are quite similar to the *RODES VI* value. No changes in murine population size, reproductive activity and morpho-physiological characteristics which may affect the population as a structural unit of the local community and ecosystem were found in the studies (Tarasov 2000; Lyubashevsky et al. 2002 a, b; Olenev and Pasechnik 2003; Orekhova and Modorov 2017). The absence of pronounced radiation-induced changes at the population level does not correspond to the risks expected from such a dose prediction. In other words, in case of bone-seeking beta emitters, doses to the bone calculated assuming the uniform radionuclide distribution in homogenous bone medium don't reflect bone marrow exposure and overestimate considerably the body-average dose, which leads to excessive conservatism. Thus, the problem of the discrepancy between the observed radioecological effects and the accumulated doses at the EURT (that caused protracted scientific discussions) (Shishkina et al. 2021a) may be solved with the help of the adequate dosimetry. This example indicates the importance of taking bone microarchitecture into account, as, for example, it was implemented in *SPDS*.

**Further direction of bone marrow dosimetry for rodents**

Limb bones, including femur, present only a part of the murine skeleton. Additionally, the main hematopoietic area includes spine (20-32% of active marrow), skull (11-20 % of active marrow) as well as pelvic bones (9-13% of active marrow) (Shaposhnikov 1979). Therefore, to get accurate estimate of the skeleton-average dose factor, it is necessary to perform the modeling of all these sites. And the next step of dosimetric modeling of bone marrow exposure will be the development/elaboration of computation phantoms of the sites mentioned above.

According to Shishkina et al. (2021b) and Volchkova et al. (2022), the main factors of influence on $DF_{Sr-90}(BM \leftarrow S)$ for small-sized bones are: 1) the surface area (depending on linear dimensions) where radiation losses are possible; and 2) the source-to-detector mass ratio (proportional to *BV/TV*). Therefore, it is important to specify both

bone geometry and microarchitecture parameters for the site-specific computational phantoms. Taking into account smaller linear dimensions of pelvic and skull bones (comparing with femur), which are very thin, preliminary one can expect greater energy losses from the volume of such bones. And, as a result, the skeleton-average $DF_r(BM \leftarrow S)$ may be smaller than that calculated for femur.

Another unsolved issue is the lack of sufficient data to create adequate phantoms of juvenile animals (<5 weeks). And the problem is not in the absence of morphometric data but in the daily morphometric changes of bones in the early period of development. Therefore, it would be reasonable to create a phantom of a newborn animal, and then interpolate the values of dose coefficients obtained to the age interval between the newborns and the growing.

## Conclusions

The study demonstrates the feasibility and appropriateness of application of the *SPSD*-approach elaborated for humans to non-human mammals. The dose factors to convert the $^{89,90}$Sr activity concentrations in a bone tissue into units of the dose rate absorbed in the femur bone marrow of growing (5-8 weeks) and adult (>8 weeks) laboratory animals (*C57BL/6*, *C57BL/6J*, *BALB/c*, *BALB/cJ*) were estimated as follows:

- $DF_{Sr-90}(BM \leftarrow TBV + CBV)$ is equal to 1.75±0.42 and 2.57±0.93 (μGy day$^{-1}$)/ (Bq g$^{-1}$) for growing and adults, respectively;
- $DF_{Sr-89}(BM \leftarrow TBV + CBV)$ is equal to 1.08±0.27 and 1.66±0.67 (μGy day$^{-1}$)/ (Bq g$^{-1}$) for growing and adults, respectively.

These results are about 2.5 times lower than those, calculated for the whole skeleton assuming the homogenous bone, where the source and target coincide.

## References

Askbrant S, Melin J, Sandalls J, Rauret G, Vallejo R, Hinton T, Cremers A, Vandecastelle C, Lewyckyj N, Ivanov YA, Firsakova SK, Arkhipov NP, Alexakhin RM. (1996) Mobility of radionuclides in undisturbed and cultivated soils in Ukraine, Belarus and Russia six years after the Chernobyl fallout. J Environ Radioact. 31(3):287–312. https://doi.org/10.1016/0265-931X(95)00054-E

Avramenko MI, Averin AN, Drozhko EG, Glagolenko YuV, Loboiko BG, Mokrov YuG, Romanov GN, Kotov ES, Filin FP (1997) Accident of 1957 Evaluation of explosion parameters and analysis of characteristics of radiation contamination of the territory. Issues of Radiats. Safety. 3:18-28 (in Russian)

Bagi CM, Berryman E, Moalli MR (2011) Comparative Bone Anatomy of Commonly Used Laboratory Animals: Implications for Drug Discovery. Comparative Medicine. 61 (1): 76 - 85

Bitar A, Lisbona A, Thedrez P, Sai Maurel C, Le Forestier D, Barbet J, Bardiès M (2007). A voxel-based mouse for internal dose calculations using Monte Carlo simulations (MCNP). Physics in Medicine and Biology. 52: 1013-1025. 10.1088/0031-9155/52/4/010

Boggs DR (1984) The total marrow mass of the mouse: a simplified method of measurement. Am J Hematol. 16(3):277-286. doi:10.1002/ajh.2830160309

Bouxsein ML, Boyd SK, Christiansen BA, Guldberg RE, Jepsen KJ, Müller R (2010) Guidelines for Assessment of Bone Microstructure in Rodents Using Micro - Computed Tomography. J Bone Miner Res. 25(7): 1468-1486. doi: 10.1002/jbmr.141.

Broulík PD, Raška I, Brouliková K (2013) Prolonged overdose of all-trans retinoic acid enhances bone sensitivity in castrated mice. Nutrition. 29(9):1166-1169. doi: 10.1016/j.nut.2013.03.011.

Brown JE, Alfonso B, Avila R, Beresford NA, Copplestone D, Hosseini A (2016) A new version of the ERICA tool to facilitate impact assessments of radioactivity on wild plants and animals. J Environ Radioact. 153: 141-148. https://doi.org/10.1016/j.jenvrad.2015.12.011

Cao JJ, Sun L, Gao H (2010) Diet-induced obesity alters bone remodeling leading to decreased femoral trabecular bone mass in mice. Ann N Y Acad Sci. 1192:292-7. doi: 10.1111/j.1749-6632.2009.05252.x.

Chesser RK, Sugg DW, Lomakin M.D, Van Den Bussche RA, Dewoody JA, Jagoe CH, Dallas CE, Whicker FW, Smith MH, Gaschak SP, Chizhevsky IG, Lyabik VV, Buntova EG, Holloman K, Baker RJ (2000) Concentrations and dose rate estimates of 134,137Cs and 90Sr in small mammals at Chornobyl, Ukraine. Environ Toxicol Chem. 19: 305–312. https://doi.org/10.1002/etc.5620190209

Chiang S-S, Pan T-M (2011) Antiosteoporotic Effects of Lactobacillus-Fermented Soy Skim Milk on Bone Mineral Density and the Microstructure of Femoral Bone in Ovariectomized Mice. J Agric Food Chem. 59(14): 7734 - 7742. doi: 10.1021/jf2013716

Dahl H, Eide DM, Tengs T, Duale N, Kamstra JH, Oughton DH, Olsen AK (2021) Perturbed transcriptional profiles after chronic low dose rate radiation in mice. PLoS One. 16(8):e0256667. doi: 10.1371/journal.pone.0256667

Degteva MO, Shagina NB, Vorobiova MI, Shishkina EA, Tolstykh EI, Akleyev AV (2016) Contemporary understanding of radioactive contamination of the Techa River in 1949–1956. Radiat. Biology. Radioecology. 85 (5): 532-534 (in Russian).

Degteva MO, Tolstykh EI, Shishkina EA, Sharagin PA, Zalyapin VI, Volchkova AYu, Smith MA, Napier BA (2021) Stochastic parametric skeletal dosimetry model for humans: General approach and application to active marrow exposure from bone-seeking beta-particle emitters. PLoS ONE. 16(10):e0257605.. doi: 10.1371/journal.pone.0257605

Doucette CR, Horowitz MC, Berry R, MacDougald OA, Anunciado-Koza R, Koza RA, Rosen CJ (2015) A High Fat Diet Increases Bone Marrow Adipose Tissue (MAT) But Does Not Alter Trabecular or Cortical Bone Mass in C57BL/6J Mice. J Cell Physiol. 230(9):2032-7. doi: 10.1002/jcp.24954.

Dubrovsky AM, Nyman JS, Uppuganti S, Chmiel KJ, Kimmel DB, Lane NE (2020) Bone Strength/Bone Mass Discrepancy in Glucocorticoid-Treated Adult Mice. JBMR Plus. 21;5(3):e10443. doi: 10.1002/jbm4.10443.

Epp ER, Woodard HQ, Weiss H (1959) Energy Absorption by the Bone Marrow of the Mouse Receiving Whole-Body Irradiation with 250-Kv X-Rays or Cobalt-60 Gamma Rays. Radiation Research. 11(2), 184. doi:10.2307/3570657

Fesenko S (2019) Review of radiation effects in non-human species in areas affected by the Kyshtym accident. J Radiol Prot. (1):R1-R17. doi: 10.1088/1361-6498/aafa92.

Gileva EA (2002) Chromosomal instability in rodents from the EURT territory: interspecies comparison. Radiats Biol Radioecol. 42(6):665-8. (In Russian).

Glatt V, Canalis E, Stadmeyer L, Bouxsein ML (2007) Age-related changes in trabecular architecture differ in female and male C57BL/6J mice. J Bone Miner Res. 22(8):1197-207. doi: 10.1359/jbmr.070507.

ICRP (2002) Basic Anatomical and Physiological Data for Use in Radiological Protection Reference Values. ICRP Publication 89. Ann. ICRP 32(3-4)

ICRP (2008). Environmental protection: the concept and use of Reference Animals and Plants. ICRP Publication 108. Ann. ICRP 38(4–6).

Ilyenko AI (1974) Concentration of radioisotopes by animals and their influence on the population. Nauka Press, Moscow (in Russian).

Iversen CM, McCormack ML, Powell AS, Blackwood CB, Freschet GT, Kattge J, Roumet C, Stover DB, Soudzilovskaia NA, Valverde-Barrantes OJ, van Bodegom PM, Violle C (2017) Viewpoints: A global Fine-Root Ecology Database to address belowground challenges in plant ecology. New Phytologist. 215: 15-26. https://doi.org/10.1111/nph.14486.

Izrael YA (2013) Atlas of the East Ural and Karachay radioactive trace including forecast up to 2047. IGCE Roshydromet and RAS, Moscow (in Russian)

Keenan MA, Stabin MG, Segars WP, Fernald MJ (2010) RADAR realistic animal model series for dose assessment. *J Nucl Med*. 51(3):471-476. doi:10.2967/jnumed.109.070532

Kramer R, Cassola VF, Vieira JW, Khoury HJ, de Oliveira Lira CAB, Robson Brown K (2012) Skeletal dosimetry based on μCT images of trabecular bone: update and comparisons. Phys Med Biol. 57(12):3995–4021. doi: 10.1088/0031-9155/57/12/3995

Locatelli M, Miloudi H, Autret G, Balvay D, Desbrée A, Blanchardon E, Bertho JM (2017) RODES software for dose assessment of rats and mice contaminated with radionuclides. J Radiol Prot. 37(1):214-229. doi: 10.1088/1361-6498/aa58aa

Lyubashevsky NM, Pashnina IA, Tarasov OV (2002b) Assessment of environmental health in the vicinity of the city of Ozersk (bioindication data). EURT-45: Regional Scientific and Practical Conference, Ozersk Chelyabinsk region, 26-27 Sept. 2002. Ozersk, VRB Publisher. pp 167-187 (in Russian)

Lyubashevsky NM, Starichenko VI, Gileva EA, Evdokimov NG, Orekhova NA, Pashnina MA, Rasina LN, Sineva NV, Tarasov OV, Yalkovskaya LE (2002a) New data on population-genetic radioadaptation of small mammals on EURT. In proceedings of International Scientific Conference “Ecological problems of mountain territories” (June 18-20, 2002). Yekaterinburg. pp 244-249 (in Russian)

Ma H, Turpeinen T, Silvennoinen M, Torvinen S, Rinnankoski-Tuikka R, Kainulainen H, Timonen J, Kujala UM, Rahkila P, Suominen H (2011) Effects of diet-induced obesity and voluntary wheel running on the microstructure of the murine distal femur. Nutr Metab (Lond). 8(1):1. doi: 10.1186/1743-7075-8-1..

Malinovsky G, Yarmoshenko I, Zhukovsky M, Starichenko V, Modorov M (2013) Strontium biokinetic model for mouse-like rodent. J Environ Radioact. 118:57-63. doi: 10.1016/j.jenvrad.2012.11.003

Malinovsky GP, Yarmoshenko IV, Zhukovsky MV, Starichenko VI, Chibiryak MV (2014) Contemporary radiation doses to murine rodents inhabiting the most contaminated part of the EURT. J Environ Radioact. 129:27-32. doi: 10.1016/j.jenvrad.2013.11.008.

Martín-Badosa E, Amblard D, Nuzzo S, Elmoutaouakkil A, Vico L, Peyrin F (2003a) Excised bone structures in mice: imaging at three-dimensional synchrotron radiation micro CT. Radiology. 229(3):921-8. doi: 10.1148/radiol.2293020558.

Martín-Badosa E, Elmoutaouakkil A, Nuzzo S, Amblard D, Vico L, Peyrin F (2003b) A method for the automatic characterization of bone architecture in 3D mice microtomographic images. Comput Med Imaging Graph. 27(6):447-58. doi: 10.1016/s0895-6111(03)00031-4.

Mikhailovskaya LN, Modorov MV, Pozolotina VN, Antonova EV (2019) Heterogeneity of soil contamination by 90Sr and its absorption by herbaceous plants in the East Ural Radioactive Trace area. Sci Total Environ. 651(Pt 2):2345-2353. doi: 10.1016/j.scitotenv.2018.10.119.

Modorov MV (2014) Radiation doses and allozyme variability in the population of the northern red-backed vole (Clethrionomys rutilus) from the east urals radioactive trace zone. Genetika. 50(2):181-8 (in Russian).

Molchanova I, Mikhailovskaya L, Antonov K, Pozolotina V, Antonova E (2014) Current assessment of integrated content of long-lived radionuclides in soils of the head part of the East Ural Radioactive Trace. J Environ Radioact. 138:238-48. doi: 10.1016/j.jenvrad.2014.09.004.

Molchanova I, Pozolotina V, Karavaeva E, Mikhaylovskaya L, Antonova E (2009) Radioactive inventories within the East-Ural radioactive state reserve on the Southern Urals. Radioprotection. 44 (5): 747–757. https://doi.org/10.1051/radiopro/20095136.

Olenev GV, Pasichnik NM (2003) Ecological Analysis of Spleen Hypertrophy in Cyclomorphic Rodents Taking into Account the Type of Ontogeny. Russian Journal of Ecology 34: 188–197.

Orekhova NA, Modorov MV (2017) East Urals Radioactive Trace: Dose-dependent functional-metabolic effects in the myocardium of the pygmy wood mouse (Apodemus uralensis) taking into account population size. J Environ Radioact. 175-176, 15-24. doi: 10.1016/j.jenvrad.2017.04.005

Orekhova NA, Modorov MV, Davydova YA (2019) Structural-functional modifications of the liver to chronic radioactive exposure in pygmy wood mouse (Apodemus uralensis) within the East-Urals Radioactive Trace. J Environ. Radioact. 199-200, 25-38. doi: 10.1016/j.jenvrad.2019.01.002.

Papageorgiou M, Föger-Samwald U, Wahl K, Kerschan-Schindl K, Pietschmann P (2020) Age- and Strain-Related Differences in Bone Microstructure and Body Composition During Development in Inbred Male Mouse Strains. Calcif Tissue Int 106, 431–443. https://doi.org/10.1007/s00223-019-00652-8

Povinec PP, Aarkrog A, Buesseler KO, Delfanti R, Hirose K, Hong G-H, Ito T, Livingston HD, Nies H, Noshkin VE, Shima S, Togawa O (2005) $^{90}$Sr, $^{137}$Cs and $^{239,240}$Pu concentration surface water time series in the Pacific and Indian Oceans - WOMARS results. J Environ. Radioact. 81: 63-87. doi: 10.1016/j.jenvrad.2004.12.003

Shaposhnikov VL (1979) Distribution of the bone marrow cells in the skeleton of mice. Biull Eksp Biol Med. 87(5):483-485 (in Russian)

Sharagin PA, Shishkina EA, Tolstykh EI, Volchkova AY, Smith MA, Degteva MO (2018) Segmentation of hematopoietic sites of human skeleton for calculations of dose to active marrow exposed to bone-seeking radionuclides. Proceedings of the RAD 2018 Conference; 2018; Macedonia, Ohrid. pp. 154–158. doi: 10.21175/RadProc.2018.33

Sharagin PA, Tolstykh EI, Shishkina EA, Napier BA, Smith MA, Degteva MO (2021) Dosimetric modeling of bone for bone-seeking beta-emitting radionuclides: size parameters and segmentation. Proceedings of the international scientific conference “Modern problems of radiobiology – 2021, Minsk, 2021”. Publisher: Information and Computing Center of the Ministry of Finance of the Republic of Belarus, Minsk, pp. 200-204 (in Russian)

Shishkina E, Zalyapin V, Timofeev YS, Degteva M, Smith M, Napier B (2018) Parametric stochastic model of bone structures to be used in computational dosimetric phantoms of human skeleton. RAD Association Journal. 3(2): 133-137 http://dx.doi.org/10.21175/RadJ.2018.02.022

Shishkina EA, Sharagin PA, Volchkova AYu (2021b) Analytical description of dose forming in bone marrow from $^{90}$Sr incorporated in calcified tissues. Journal of Radiation Safety Issues. 103 (3): 72-82 (in Russian).

Shishkina EA, Starichenko VI, Valeeva ER, Lyubashevsky NM, Modorov MV (2021a) Assessment of herb field mouse (Sylvaemus uralensis) migration in the area of the east urals radioactive trace using measurements of bone-seeking $^{90}$Sr. J Environ Radioact. 237:106663. doi: 10.1016/j.jenvrad.2021.106663.

Shishkina EA, Timofeev YS, Volchkova AY, Sharagin PA, Zalyapin VI, Degteva MO, Smith MA, Napier BA (2020) Trabecula: A Random Generator of Computational Phantoms for Bone Marrow Dosimetry. Health Phys. 118(1):53-59. doi: 10.1097/HP.0000000000001127

Soppera N, Bossant M, Dupont E (2014) JANIS 4: An Improved Version of the NEA Java - based Nuclear Data Information System. Nuclear Data Sheets. 120.: 294-296 doi 10.1016/j.nds.2014.07.071.

Stabin MG, Peterson TE, Holburn GE, Emmons MA (2006) Voxel-based mouse and rat models for internal dose calculations. J. Nucl. Med. 47 (4): 655–659.

Starichenko VI, Lyubashevskiy NM, Modorov MV, Chibiryak MV (2014) Skeletal $^{90}$Sr as a Marker of Migration Activity of Murine Rodents in the Zone of the Eastern Ural Radioactive Trace. Russ J Ecol. 45(3): 231–241 https://doi.org/10.1134/S1067413614030126

Starichenko VI (2004) Accumulation of $^{90}$Sr in the bone tissue of the northern mole vole, living in the head part of the East Ural Radioactive Trace. Radiats Biol Radioecol. 44(3): 346–350 (in Russian).

Taketa ST, Carsten AL, Cohn SH, Atkins HL, Bond VP (1970) Active bone marrow distribution in the monkey. Life Sci. 8;9(3):169-74. doi: 10.1016/0024-3205(70)90310-3.

Tamasi JA, Vasilov A, Shimizu E, Benton N, Johnson J, Bitel CL, Morrison N, Partridge NC (2013) Monocyte chemoattractant protein-1 is a mediator of the anabolic action of parathyroid hormone on bone. J Bone Miner Res. 28(9):1975-86. doi: 10.1002/jbmr.1933.

Tarasov OV (2000) Radioecology of terrestrial vertebrates of the East Ural radiation reserve. PhD theses, Institute of Plant and Animal Ecology, Ural Branch of the Russian Academy of Sciences (IPAE) (in Russian).

Tolstykh, EI, Sharagin PA, Shishkina EA, Degteva MO, Napier BA, Smith MA (2021) Dosimetric modeling of red bone marrow exposure from $^{89,90}$SR: resolving age-dependent trabecular bone parameters. Proceedings of the international scientific conference “Contemporary issues of radiobiology – 2021 (September23-24, 2021, Gomel)”. Publisher: IVC Minfina, Minsk, pp. 176-179 (in Russian).

Turner CH, Hsieh YF, Müller R, Bouxsein ML, Baylink DJ, Rosen CJ, Grynpas MD, Donahue LR, Beamer WG (2000) Genetic regulation of cortical and trabecular bone strength and microstructure in inbred strains of mice. J Bone Miner Res. 15(6):1126-31. doi: 10.1359/jbmr.2000.15.6.1126.

Verdelis K, Lukashova L, Atti E, Mayer-Kuckuk P, Peterson MG, Tetradis S, Boskey AL, van der Meulen MC (2011) MicroCT morphometry analysis of mouse cancellous bone: intra- and inter-system reproducibility. Bone. 49(3):580-7. doi: 10.1016/j.bone.2011.05.013.

Voide R, van Lenthe GH, Müller R (2008) Bone morphometry strongly predicts cortical bone stiffness and strength, but not toughness, in inbred mouse models of high and low bone mass. J Bone Miner Res. 23(8):1194-203. doi: 10.1359/jbmr.080311.

Volchkova AY, Sharagin PA, Shishkina EA (2022) Internal bone marrow dosimetry: the effect of the exposure due to $^{90}$Sr incorporated in the adjacent bone segments. Bulletin of the South Ural State University Ser Mathematical Modelling, Programming & Computer Software (Bulletin SUSU MMCS) (in press).

Wu Y, Liu J, Guo H, Luo Q, Yu Z, Liao E, Zu X (2013) Establishment of OPG Transgenic Mice and the Effect of OPG on Bone Microarchitecture. Int J Endocrinol. 2013:125932. doi: 10.1155/2013/125932.

Xiang A, Kanematsu M, Kumar S, Yamashita D, Kaise T, Kikkawa H, Asano S, Kinoshita M (2007) Changes in micro-CT 3D bone parameters reflect effects of a potent cathepsin K inhibitor (SB-553484) on bone resorption and cortical bone formation in ovariectomized mice. Bone. 40(5):1231-7. doi: 10.1016/j.bone.2007.01.010.

Zalyapin V, Timofeev Yu, Shishkina E (2018) A parametric stochastic model of bone geometry. Bulletin of the South Ural State University Ser Mathematical Modelling, Programming & Computer Software (Bulletin SUSU MMCS). 11:44–57 (in Russian). https://doi.org/10.14529/mmp180204

Zankl M, Becker J, Lee C, Bolch WE, Yeom YS, Kim CH (2018) Computational phantoms, ICRP/ICRU, and further developments. Ann ICRP. 47(3-4):35-44. doi: 10.1177/0146645318756229.

## Figure Captions

**Fig. 1** Creation of computational phantom of murine femur

Table 1 Mass fraction of chemical composition and medium densities

| Element N | Element | Mass fraction | |
|---|---|---|---|
| | | Bone marrow | Bone |
| 1 | H | 0.097 | 0.035 |
| 6 | C | 0.386 | 0.16 |
| 7 | N | 0.037 | 0.042 |
| 8 | O | 0.456 | 0.445 |
| 11 | Na | 0.001 | 0.003 |
| 12 | Mg | 0.002 | 0.002 |
| 15 | P | 0.018 | 0.095 |
| 16 | S | 0.002 | 0.003 |
| 20 | Ca | — | 0.215 |
| 26 | Fe | 0.0009 | — |
| Density, g $cm^{-3}$ | | 0.98 | 1.57 |

Table 2 The literature sources and information available: gray cells indicate the presence of information on the parameter studied in the paper (m- male; f- female)

| Source | Strain | Sex | Age range, weeks | Number of animals | Parameter studied | | | | | |
|---|---|---|---|---|---|---|---|---|---|---|
| | | | | | $L$ | $D$ | $BV/TV$ | $Tb.Th$ | $Tb.Sp$ | $Ct.Th$ |
| Dubrovsky et al. 2020 | BALB/cJ | m | 21 - 30 | 20 | | | | | | |
| Doucette et al. 2015 | C57BL/6J | m | 14 - 15 | 10 | | | | | | |
| Xiang et al. 2007 | BALB/c | f | 7 - 9 | 10 | | | | | | |
| Cao et al. 2010 | C57BL/6 | m | 13 - 14 | 11 | | | | | | |
| Martín-Badosa et al. 2003a | C57BL/6J | m | 16 | 20 | | | | | | |
| Martín-Badosa et al. 2003b | C57BL/6J | M | 17 - 18 | 8 | | | | | | |
| Glatt et al. 2007 | C57BL/6J | m&f | 4 - 87 | 232 | | | | | | |
| Voide et al. 2008 | C57BL/6J | m&f | 11 - 15 | 20 | | | | | | |
| Chiang and Pan 2011 | C57BL/6J | F | 33 - 34 | 8 | | | | | | |
| Verdelis et al. 2011 | C57BL/6 | m | 11 - 12 | 6 | | | | | | |
| Ma et al. 2011 | C57BL/6J | m | 28 | 10 | | | | | | |
| Wu et al. 2013 | C57BL/6J | f | 17 - 20 | 6 | | | | | | |
| Bagi et al. 2011 | C57BL/6 | m&f | 3 - 5 | 12 | | | | | | |
| Tamasi et al. 2013 | C57BL/6 | m | 23 | 12 | | | | | | |
| Turner et al. 2000 | C57BL/6 | f | 15 - 16 | 25 | | | | | | |

Table 3 Parameters of bone geometry model for computational phantoms of growing and adult femur of laboratory animals (C57BL/6, C57BL/6J, BALB/c, BALB/cJ)

| Age | Parameters | | | | | |
|---|---|---|---|---|---|---|
| | $l$, mm | $d$, mm | $\widehat{BV/TV}$ | $\widehat{Tb.Th}$, mm | $\widehat{Tb.Sp}$, mm | $\widehat{Ct.Th}$, mm |
| Growing | 13±1 | 1.5±0.2 | 0.13±0.05 | 0.04±0.01 | 0.25±0.03 | 0.09±0.02 |
| Adults | 16.0±0,8 | 1.5±0.2 | 0.12±0.09 | 0.04±0.02 | 0.25±0.08 | 0.19±0.08 |

Table 4 Dose factors $DF_r(BM \leftarrow S)$ for $^{90}$Sr and $^{89}$Sr incorporated in *TBV* and *CBV* (*S*=*TBV* or *S*=*CBV*) to convert the radionuclide specific activity into the dose rate in the *BM*; *rmsd* – root mean square deviation

| Age | $DF_r(BM \leftarrow S)$ ± *rmsd*, (μGy day$^{-1}$) per (Bq g$^{-1}$) | | | | | |
|---|---|---|---|---|---|---|
| | *r*=$^{90}$Sr | | | *r*=$^{89}$Sr | | |
| | *S=TBV* | *S=CBV* | *S*[a]*=TBV+CBV* | *S=TBV* | *S=CBV* | *S*[a]*=TBV+CBV* |
| Growing | 0,81±0,30 | 0,93±0,12 | 1,75±0,42 | 0,48±0,18 | 0,61±0,09 | 1,08±0,27 |
| Adults | 0,67±0,36 | 1,90±0,56 | 2,57±0,93 | 0,38±0,25 | 1,28±0,42 | 1,66±0,67 |

[a] assuming uniform radionuclide distribution within all bone structures

Table 5 Dose factors calculated for adults using different approaches to convert Sr isotope activity concentrations in a source (*S*) into dose rates in a target (*T*). 90% confidence interval [90%CI] bordered the range of possible individual variations

| Isotopes | $DF_{Sr-90}(T \leftarrow S)$, (μGy day$^{-1}$) per (Bq g$^{-1}$) | | |
|---|---|---|---|
| | *SPSD*-approach, femur<br>*S=TBV+CBV*<br>*T=BM* | *«ERICA Tool2»*<br>*S*= whole body<br>*T*=whole body | *« RODES VI»*<br>*S*=homogenous skeleton<br>*T*= homogenous skeleton |
| $^{90}$Sr | 2,6 [1.3 – 4.0] | 12,9 | 6,5 |
| $^{89}$Sr | 1,7 [0.8 – 2.7] | 7,5 | 3,6 |

Table 6 The group-average data on $^{90}$Sr activity concentration (*A*) in the murine bones (according to Shishkina et al. 2021a) and corresponding dose rates in bone marrow due to internal exposure to $^{90}$Sr. The 90%CI for the dose rate reflects the overall individual variability of the activity concentrations and dose factors

| Initial deposition density of sampling site | Status of maturity | N | A±st.dev, Bq g$^{-1}$ (Wet weight) | $\dot{D}$ [90%CI], μGy day$^{-1}$ |
|---|---|---|---|---|
| 37 kBq m$^{-2}$ | growing | 21 | 0.6±0.2 | 1.1 [0.4-2.0] |
| | adults | 48 | 1.0±0.6 | 1.9 [0.3-3.8] |
| 74-3700 kBq m$^{-2}$ | growing | 299 | 18±1 | 34 [16 - 55] |
| | adults | 75 | 18±3 | 46 [12 - 87] |
| 3.7 -37 MBq m$^{-2}$ | growing | 76 | 52±9 | 98 [43 - 162] |
| | adults | 54 | 44±8 | 84 [21 - 158] |

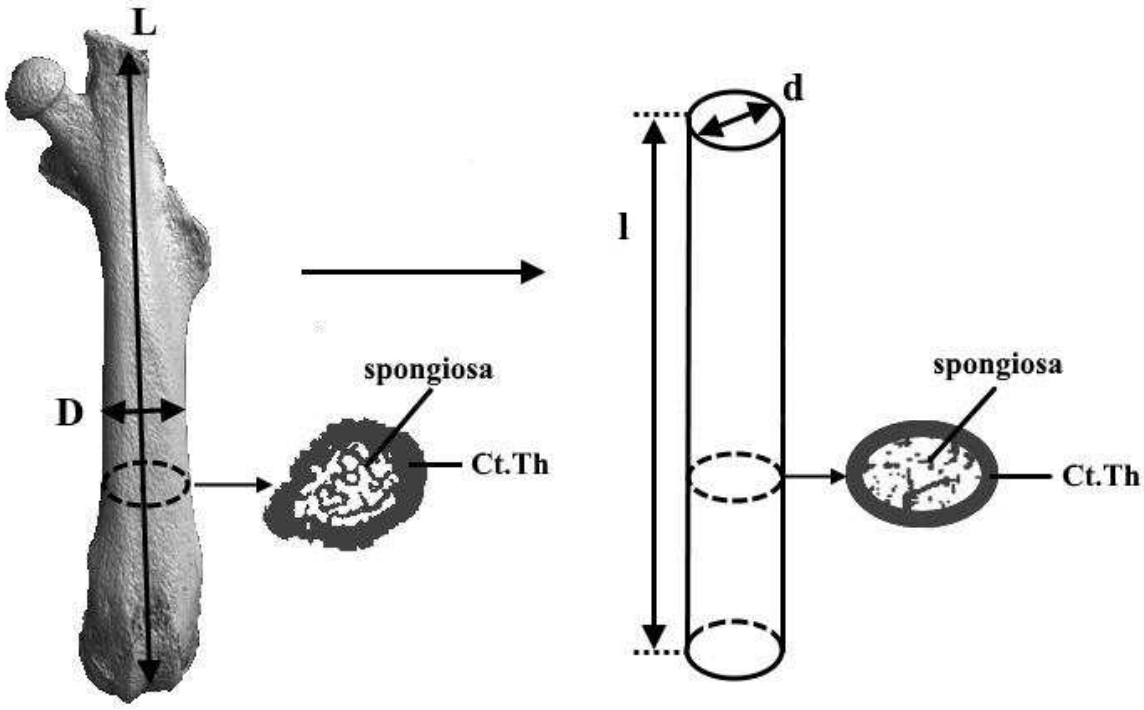


**Fig. 1** Creation of computational phantom of murine femur

# Supplementary Files

This is a list of supplementary files associated with this preprint. Click to download.

- SupplementaryInformation.xlsx